Letter

# Manifolds of exceptional points and effective Zeno limit of an open two-qubits system

Vladislav Popkov [1,2], Carlo Presilla [3,4] and Mario Salerno [5]

[1]*Faculty of Mathematics and Physics, University of Ljubljana, Jadranska 19, SI-1000 Ljubljana, Slovenia*

[2]*Bergisches Universität Wuppertal, Gauss Strasse 20, D-42097 Wuppertal, Germany*

[3]*Dipartimento di Matematica, Sapienza Università di Roma, Piazzale A. Moro 5, I-00185 Rome, Italy*

[4]*Istituto Nazionale di Fisica Nucleare, Sezione di Roma 1, I-00185 Rome, Italy*

[5]*Dipartimento di Fisica "E. R. Caianiello," Università di Salerno, Via Giovanni Paolo II, I-84084 Fisciano (SA), Italy*

(Received 17 December 2024; accepted 6 May 2025; published 19 May 2025)

We analytically investigate the Liouvillian exceptional point manifolds (LEPMs) of a two-qubits open system, where one qubit is coupled to a dissipative polarization bath. Exploiting a $Z_2$ symmetry, we block diagonalize the Liouvillian and show that one symmetry block yields two planar LEPMs while the other one exhibits a more intricate, multisheet topology. The intersection curves of these manifolds provide a phase diagram for effective Zeno transitions at small dissipation. These results are consistent with a perturbative extrapolation from the strong Zeno regime. Interestingly, we find that the fastest relaxation to the nonequilibrium steady state occurs on LEPMs associated with the transition to the effective Zeno regime.

DOI: 10.1103/PhysRevA.111.L050202

*Introduction.* A strong spectral response to perturbations occurs in open quantum systems at their branch-point singularities, the so-called exceptional points (EPs) [1–3]. This phenomenon can be used for sensing [4,5], hardware encryption [6], optimizing performance of quantum thermal machines [7], realizing a multipoint switch between modes in photonic systems [8], and other applications [9].

In classical and semiclassical systems that ignore quantum jumps, EPs are typically associated with degeneracies of non-Hermitian Hamiltonians, and many theoretical aspects are well understood. At the quantum level, EPs appear in Markovian open systems, i.e., quantum dynamical semigroups whose time evolution obeys a Lindblad master equation, with a time-independent Liouvillian superoperator as the generator [10–12]. In these systems, exceptional points of the Liouvillian (LEPs) occur in the parameter space where Liouvillian eigenvalues and eigenvectors coalesce.

In contrast to the EPs of non-Hermitian Hamiltonians, the LEPs include quantum jumps that reflect the open nature of the systems and allow a comprehensive understanding of their dynamics in interactions with the environment [13]. Moreover, LEPs provide information that is crucial in the analysis of rapidly decaying states in systems subject to decoherence [14].

The distribution of LEPs driven by the interplay between non-Hermitian dynamics and dissipation gives rise to Liouvillian exceptional point manifolds (LEPMs) in the parameter space. Understanding these manifolds is crucial for controlling the system, such as optimizing sensing applications near LEPs by tuning the system parameters. Conversely, operating in regions where LEPs do not occur is essential for applications that require stability, such as quantum computing [15]. Additionally, the knowledge of LEPMs helps to identify the parameter regions where the transition to the Zeno regime can be achieved with minimal dissipative coupling to the environment.

Except for a few solvable cases involving two- [16] and three-level systems [17], LEPMs, to our knowledge, are practically unexplored [18] (we discard all cases for which LEPs reduce to EPs of non-Hermitian Hamiltonians as for example in Ref. [18]).

The aim of the present Letter is to provide a full analytical characterization of all the LEPMs of a two-qubits system and to show how LEPMs can be used to optimize the phase transitions of the system to an effective Zeno regime by keeping the dissipative couplings with the environment as small as possible.

In particular, we consider two $XYZ$ Heisenberg spins 1/2 interacting with exchange anisotropies $J \equiv (J_x, J_y, J_z)$ and coupled to a dissipative polarization bath through one of the two spins only (see Fig. 1 for a scheme and Refs. [19–22] for experimental realizations of a spin chain as well as of a polarization bath). The parameter space is three dimensional and consists, without loss of generality, of the two parameters, $\gamma = J_y/J_x$, $\Delta = J_z/J_x$ (i.e., we work in units of $J_x = 1$), for the Hamiltonian and one parameter, $\Gamma$, fixing the strength of the dissipative coupling to the bath. We take advantage of a $Z_2$ symmetry to block diagonalize the Liouvillian superoperator into two blocks, one of which is independent of $\Delta$.

Using this symmetry, we derive polynomial equations that describe all the LEPMs. We show that, by restricting only to real values of the parameters, for the $\Delta$-independent block, LEPMs reduce to two planes, $\Gamma = 8$ and $\Gamma = 8\gamma$, while for the other block, they exhibit more intricate topologies with a number of sheets (branches) varying between one and six, depending on parameter values.

Quite remarkably, from the intersection curves of some of these surfaces, it is possible to derive a phase diagram in the $(\gamma, \Delta)$ plane for effective Zeno transitions occurring at small dissipation. Also notable is the fact that the fastest relaxation to the nonequilibrium steady state (NESS) from an initial perturbation occurs precisely at the LEPMs that lie at

 

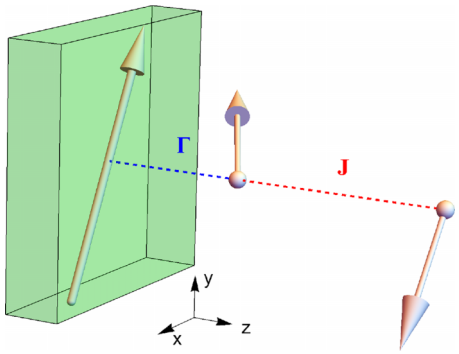


FIG. 1. An open two-qubits system is schematized as two $XYZ$ Heisenberg spins 1/2 interacting via anisotropic exchange energies of strength $J \equiv (J_x, J_y, J_z)$. The system is coupled to a polarization dissipative bath (green box with a large arrow inside) only through one of the two spins. The red and blue dashed lines represent the Heisenberg exchange interaction between the two spins and the coupling $\Gamma$ between the first spin and the bath, respectively. Small spheres indicate the sites on which the spins are located.

the boundary with the effective Zeno regime. These results are in agreement with a perturbative calculation that extrapolates the strong Zeno regime to small dissipations.

*Two-qubits model and Liouvillian symmetry.* We consider an open system of two qubits undergoing an anisotropic exchange interaction of strength $(1, \gamma, \Delta)$ in the $(x, y, z)$ directions, respectively, and a Markovian dissipation of strength $\Gamma$ acting only on qubit 1. The reduced density matrix $\rho$ of the system evolves in time according to the Lindblad master equation

$$\frac{\partial \rho}{\partial t} = \mathcal{L}\rho \equiv -i[H, \rho] + \Gamma\big(L\rho L^\dagger - \tfrac{1}{2}(L^\dagger L\rho + \rho L^\dagger L)\big), \quad (1)$$

with jump operator $L = \sigma^+ \otimes I_2$, $I_n$ being the $n \times n$ identity matrix, and Hamiltonian

$$H = \sigma^x \otimes \sigma^x + \gamma\, \sigma^y \otimes \sigma^y + \Delta\, \sigma^z \otimes \sigma^z. \quad (2)$$

As usual, $\sigma^\pm = (\sigma^x \pm i\sigma^y)/2$, with $\sigma^x, \sigma^y, \sigma^z$ being the Pauli matrices. Besides $J_x = 1$, we work also in units of $\hbar = 1$ so that in Eq. (1) we have $t = t_{\rm ph} J_x/\hbar$ and $\Gamma = \Gamma_{\rm ph}\hbar/J_x$, where $t_{\rm ph}$ and $\Gamma_{\rm ph}$ are the physical time and the physical dissipation strength obtained for the effective values of $\hbar$ and $J_x$. In present units the parameters $\gamma, \Delta, \Gamma$ as well as the time $t$ and the operators $H$ and $\mathcal{L}$ are dimensionless. Note also that $H = H(\gamma, \Delta)$ and $\mathcal{L} = \mathcal{L}(\gamma, \Delta, \Gamma)$. For $H = 0$, the dissipative term proportional to $\Gamma$ would result in relaxation of the first spin into the fully polarized state in the $z$ direction, namely $|\uparrow\rangle\langle\uparrow|$, where $\sigma^z|\uparrow\rangle = |\uparrow\rangle$, with a relaxation time of order $1/\Gamma$. We will find the solution of Eq. (1) by solving the associated eigenvalue problem $\mathcal{L}\rho = \lambda\rho$ in vector form [23] $\mathrm{vec}(\mathcal{L}\rho) = \mathcal{L}_{\rm vec}\mathrm{vec}(\rho) = \lambda\,\mathrm{vec}(\rho)$. The corresponding vectorized Liouvillian is given by the $16 \times 16$ matrix

$$\mathcal{L}_{\rm vec} = -iH \otimes I_4 + iI_4 \otimes H^{\rm T} + \Gamma\big(L \otimes L^* - \tfrac{1}{2}(L^\dagger L) \otimes I_4 - \tfrac{1}{2} I_4 \otimes (L^\dagger L)^{\rm T}\big). \quad (3)$$

Both the Hamiltonian $H$ and the Lindblad operator $L$ commute with the operator $\Sigma_z = \sigma^z \otimes \sigma^z$, namely,

$$[\Sigma_z, H] = 0, \quad [\Sigma_z, L] = 0. \quad (4)$$

These relations can be used to block-diagonalize the vectorized Liouvillian $\mathcal{L}_{\rm vec}$ as follows. Introduce the matrices $Q_\pm = \frac{1}{2}(I_{16} \pm \Sigma_z \otimes \Sigma_z)$ which satisfy

$$Q_+ + Q_- = I_{16}, \quad [Q_\pm, \mathcal{L}_{\rm vec}] = 0,$$
$$Q_\pm Q_\mp = 0, \quad Q_\pm \mathcal{L}_{\rm vec} Q_\mp = 0. \quad (5)$$

From these relations we have $\mathcal{L}_{\rm vec} = \mathcal{L}_+ + \mathcal{L}_-$, where $\mathcal{L}_\pm = Q_\pm \mathcal{L}_{\rm vec} Q_\pm$ are matrices of rank 8 satisfying $\mathcal{L}_\pm \mathcal{L}_\mp = 0$. The block diagonalization of the vectorized Liouvillian is then achieved as

$$\mathcal{L}_{\rm vec} = \Sigma_+ \oplus \Sigma_- = \begin{pmatrix} \Sigma_+ & 0 \\ 0 & \Sigma_- \end{pmatrix}, \quad (6)$$

where $\Sigma_\pm$ are $8 \times 8$ diagonal blocks, obtained from $\mathcal{L}_\mp = 0$ by eliminating the eight null rows and columns present in these matrices [see Supplemental Material (SM) [24] for explicit matrix elements].

*Liouvillian spectrum and LEPMs.* The full Liouvillian spectrum can be obtained by diagonalizing the blocks $\Sigma_\pm$ separately. Since the parameter $\Delta$ appears only in the lower diagonal block $\Sigma_-$ SM [24], the block diagonalization allows to separate the $\Delta$-dependent and $\Delta$-independent parts of the spectrum into two orthogonal spaces.

The secular equation for the eigenvalues of the block $\Sigma_+$ is given by $\lambda(\Gamma + \lambda)(\Gamma + 2\lambda)^2 \Lambda(\gamma, \Gamma) = 0$, where $\Lambda(\gamma, \Gamma)$ is the quartic polynomial in $\lambda$

$$\Lambda(\gamma, \Gamma) = \lambda^4 + 2\Gamma\lambda^3 + \left[8(1+\gamma^2) + \frac{5}{4}\Gamma^2\right]\lambda^2 + \left[8(1+\gamma^2)\Gamma + \frac{\Gamma^3}{4}\right]\lambda + 2[8(1+\gamma^4) + \Gamma^2 + \gamma^2(\Gamma^2 - 16)].$$

Thus, the eight $\Delta$-independent eigenvalues of $\Sigma_+$ are

$$\lambda(\gamma, \Gamma) = \left\{0, -\Gamma, -\frac{\Gamma}{2}, -\frac{\Gamma}{2}, -\frac{\Gamma}{2} \pm \frac{\sqrt{2}}{4} \times \sqrt{\Gamma^2 - 32(1+\gamma^2) \pm \sqrt{(\Gamma^2 - 64)(\Gamma^2 - 64\gamma^2)}}\right\}. \quad (7)$$

From Eq. (7) we see that these eigenvalues always have branching points at two different values of $|\Gamma|$, namely, $|\Gamma| = 8$ and $|\Gamma| = 8|\gamma|$. Apart from these, $\lambda(\gamma, \Gamma)$ has no other singular points. The remaining eight $\Delta$-dependent eigenvalues of the block $\Sigma_-$ are given by (see SM [24] for details)

$$\lambda = \tfrac{1}{2}(-\Gamma \pm \sqrt{\Gamma^2 + \xi_i}), \quad i = 1, \ldots, 4, \quad (8)$$

where $\xi_i = \xi_i(\gamma, \Delta, \Gamma)$ are the roots of the quartic polynomial

$$c_a \xi^4 + c_b \xi^3 + c_c \xi^2 + c_d \xi + c_e = 0, \quad (9)$$

with coefficients $c_a, c_b, c_c, c_d, c_e$, which depend on $\gamma, \Delta, \Gamma$, given in SM [24]. The branching points of the $\Sigma_-$ eigenvalues

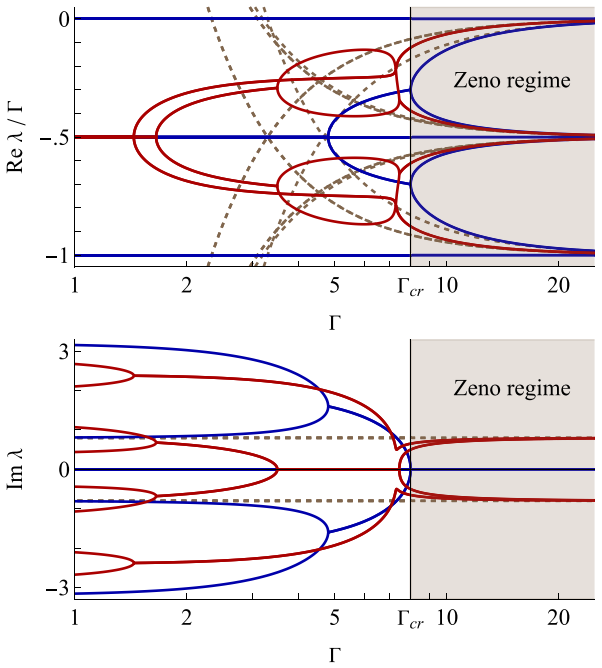


FIG. 2. Real (top panel) and imaginary (bottom panel) parts of the eigenvalues $\lambda$ of the Liouvillian operator (3) vs $\Gamma$. Red and blue lines refer to eigenvalues of the $\Sigma_+$ and $\Sigma_-$ blocks of $\mathcal{L}_{\rm vec}$, respectively. LEPs coincide with the eigenvalue branching points and correspond to broken/resumed symmetries (change of eigenvalue degeneracies). Dashed lines denote perturbative extrapolations of the eigenvalues from the strong, $\Gamma \gg \Gamma_{\rm cr}$, Zeno regime, to the low dissipation Zeno regime, $\Gamma \approx \Gamma_{\rm cr}$, with $\Gamma_{\rm cr}$ given in (11). Note the logarithmic horizontal scale and the rescaling of $\mathrm{Re}\,\lambda$ by $\Gamma$ operated in the top panel. Parameters are fixed as $\gamma = 0.6$, $\Delta = 0.4$, corresponding to point b in the bottom panel of Fig. 4.

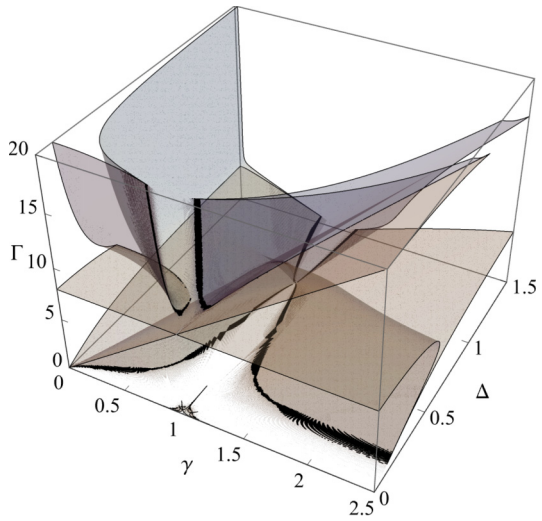


FIG. 3. Two-dimensional LEP manifolds of the two-qubits open system (1) in the three-dimensional parameter space $\{\gamma, \Delta, \Gamma\}$. Only the LEP manifolds originating from the $\Delta$-dependent block $\Sigma_-$ of the Liouvillian are shown here.

are obtained by equating to zero the discriminant of the polynomial in Eq. (9), thus leading to the following eight degree polynomial equation in the $Z = \Gamma^2$ variable

$$\sum_{i=0}^{8} a_i(X, Y) Z^i = 0, \tag{10}$$

with coefficients $a_i$ that are polynomials in $Y = \Delta^2$ with coefficients which are polynomials in $X = \gamma^2$ SM [24].

We stress that the equations determining the branching points of both the $\Sigma_+$ and $\Sigma_-$ eigenvalues depend on the squares of the parameters $\gamma, \Delta, \Gamma$. It follows that our results are invariant with respect to a change of sign of each one of these parameters. Hereafter, for simplicity, we will assume that $\gamma, \Delta, \Gamma$ are all positive [25]. Depending on the values of the parameters $\gamma$ and $\Delta$, we have LEPs, corresponding to branching points in $\mathrm{Re}\,\lambda(\Gamma)$ and $\mathrm{Im}\,\lambda(\Gamma)$ at up to $2 + 6 = 8$ different values of $\Gamma$. An example with LEPs at $2 + 5$ different values of $\Gamma$ is shown in Fig. 2, and other examples are given in SM [24]. In general, at an EP the eigenvalue coalescence goes along with an eigenvector coalescence [26], which means nondiagonalizability of the Liouvillian at any LEP. In SM [24] we provide analytic expressions of the Liouvillian eigenvectors on various LEPMs explicitly showing the characteristic Jordan block decomposition of $\Sigma_\pm$.

In the three-dimensional space of parameters $\gamma, \Delta, \Gamma$ the values of $\Gamma$ for which LEPs are found form two-dimensional manifolds $\Gamma(\gamma, \Delta)$. The LEP manifolds originating from the $\Delta$-dependent block $\Sigma_-$ of the Liouvillian are shown in Fig. 3. Due to the divergence of some manifolds in the limit $\Delta \to 0$ (see later), the plot is limited to $\Delta \geqslant 0.05$. The two manifolds originating from the $\Delta$-independent block $\Sigma_+$ of the Liouvillian, not shown in Fig. 3, correspond to the straight planes $\Gamma = 8$ and $\Gamma = 8|\gamma|$.

Aiming at Zeno limit applications, we examine the location of the LEPs with the largest $\Gamma$ value. Denoting by $\Gamma_{{\rm LEP},j}$ the $\Gamma$ coordinates of the branching points in the $(\Gamma, \lambda_j)$ plane (see Fig. 2), we define $\Gamma_{\rm cr}$ as the $\Gamma$ value beyond which all eigenvalues are analytical:

$$\Gamma_{\rm cr}(\gamma, \Delta) = \sup_j \Gamma_{{\rm LEP},j}. \tag{11}$$

The behavior of $\Gamma_{\rm cr}(\gamma, \Delta)$ is shown in Fig. 4 by a bare three-dimensional plot in the top panel and a $(\gamma, \Delta)$ diagram in the bottom panel. Remarkably, the $(\gamma, \Delta)$ plane is divided into two regions by a solid red boundary line (given parametrically in SM [24]). The region above this line is further split by the dashed line $\gamma = 1$ into two parts: the gray region $\gamma < 1$ where $\Gamma_{\rm cr} = 8$, and the green region $\gamma > 1$ where $\Gamma_{\rm cr} = 8\gamma$. In the blue region below the solid red line, $\Gamma_{\rm cr}$ corresponds to LEPs arising from eigenvalues of $\Sigma_-$ and depends on both $\gamma$ and $\Delta$. In this region $\Gamma_{\rm cr}$ increases as $\Delta$ is decreased, and diverges [see Eq. (14)] as $\Delta \to 0$, except at $\gamma = 1$; the same holds for $\gamma \to 0$. In contrast, in the gray and green regions of the phase diagram, no singularities occur and the dynamics becomes fully analytic. This analyticity allows for an expansion in $1/\Gamma$, leading to an effective near-Zeno dynamics, as explained below.

*Relaxation times near and on LEPMs.* Interestingly, we find that in the region of parameter space characterized by $\Gamma_{\rm cr} = 8$ (see Fig. 4) the fastest relaxation from an initial perturbed state to the exact NESS given in SM [24] is achieved on the $\Gamma = 8$

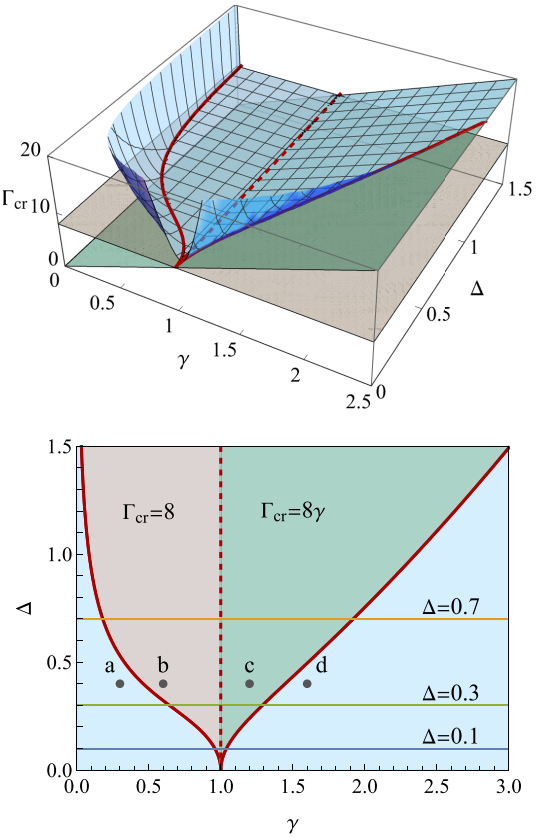


FIG. 4. Top panel: Behavior of $\Gamma_{cr}(\gamma, \Delta)$, light-blue surface with a mesh, for $\Delta \geqslant 0.05$. Within the region delimited by the red continuous line this surface coincides with the straight planes $\Gamma_{cr} = 8$ (displayed in gray) and $\Gamma_{cr} = 8\gamma$ (displayed in green). Bottom panel: Two-dimensional diagram of $\Gamma_{cr}(\gamma, \Delta)$. The detailed branching point structure of the Liouvillian eigenvalues at the point labeled b is shown in Fig. 2. The same information at points a, c, and d is provided in SM [24]. In SM [24] we also show the sections of $\Gamma_{cr}(\gamma, \Delta)$ at the planes $\Delta = 0.1$, 0.3, and 0.7 whose projections are indicated here by tiny solid lines.

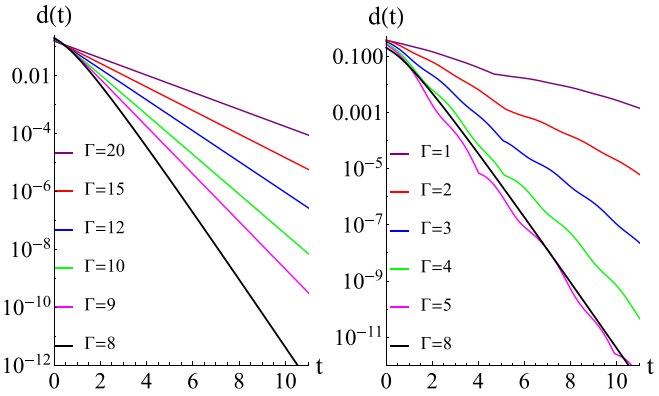


FIG. 5. Distance $d(t) \equiv \|\rho(t) - \rho_{NESS}(\gamma_f)\|_2$ vs time $t$ for rapid quenches in the parameter $\gamma$, from $\gamma_i = 0.4$ to $\gamma_f = 0.8$, on different constant-$\Gamma$ planes as indicated in the legend, for arbitrary $\Delta$. The left panel shows data for planes above the $\Gamma = 8$ LEPM, while the right panel data for planes below it.

LEPM. To show this we perform instantaneous quenches of the parameter $\gamma$ from $\gamma_i$ to $\gamma_f$ on different constant-$\Gamma$ planes, keeping $\Delta$ fixed. The quench is implemented by setting the initial condition as $\rho_i = \rho_{NESS}(\gamma_i, \Gamma)$, the exact NESS [see Eq. (S13) in SM [24]] corresponding to $\gamma_i$, for the time evolution governed by Eq. (1) with $\mathcal{L}$ corresponding to $\gamma_f$, i.e., $\mathcal{L} \equiv \mathcal{L}(\gamma_f, \Delta, \Gamma)$. To characterize the relaxation dynamics, we compute the distance between $\rho(t)$ and $\rho_{NESS}(\gamma_f)$, and plot it as a function of time. The results are shown in Fig. 5.

From the left panel, we observe that the relaxation time increases above $\Gamma = 8$. This slower relaxation is due to the onset of the quantum Zeno regime where the effective dissipation strength starts to decrease with $\Gamma$ [see Eq. (12)]. The relaxation curves in this regime are smooth and uniform, as expected due to the absence of LEPMs above $\Gamma = 8$. In contrast, below the LEPM plane, right panel, the relaxation curves develop undulations or cusps, which we attribute to interference with other LEPM branches present below the $\Gamma = 8$ plane. Just below the LEPM plane, the relaxation time decreases slightly before rapidly increasing as $\Gamma$ is reduced further. A similar behavior is observed when $\Gamma_{cr} = 8\gamma$ (see Fig. S5 in SM [24]).

*Effective near Zeno dynamics.* If the dissipation is strong, and in the absence of branching points, i.e., for $\Gamma \gg \Gamma_{cr}$, all Liouvillian eigenvalues can be calculated explicitly using a perturbative Dyson series [27]. The complete set of 16 Liouvillian eigenvalues up to order $1/\Gamma$ included is given by

$$\lambda_{0,\alpha} = \left\{0, -2\frac{\gamma_+}{\Gamma}, -\frac{\gamma_+}{\Gamma} \pm 2\Delta i\right\},$$
$$\lambda_{1,\alpha} = \left\{-\frac{\Gamma}{2}, -\frac{\Gamma}{2}, -\frac{\Gamma}{2} \pm \frac{2\gamma_-}{\Gamma}, -\frac{\Gamma}{2} \pm \frac{8\gamma}{\Gamma} \pm 2\Delta i\right\},$$
$$\lambda_{2,\alpha} = \left\{-\Gamma, -\Gamma + 2\frac{\gamma_+}{\Gamma}, -\Gamma + \frac{\gamma_+}{\Gamma} \pm 2\Delta i\right\},$$

where $\gamma_\pm = 4(1 \pm \gamma^2)$. The eigenvalues are labeled by a stripe index, numbers 0, 1, 2, and a mode index, Greek letters $\alpha$ ranging from 1 to 4 for stripes 0 and 2 and from 1 to 8 for stripe 1 (see Ref. [27]). The modes $\lambda_{0,\alpha}$ contain the NESS, corresponding to the null eigenvalue, and the slowest relaxation modes, which determine the late time evolution. On the other hand, the modes $\lambda_{1,\alpha}, \lambda_{2,\alpha}$ have large negative real parts and thus correspond to the rapid relaxation of the first spin towards the target state, namely, the qubit fully polarized along the $z$ axis. The above asymptotic expressions for Liouvillian eigenvalues are shown in Fig. 2 by dashed lines.

The theory also predicts [27] explicit analytic expressions for the Liouvillian eigenvectors as well as an effective near Zeno dynamics. Namely, while the first spin relaxes towards the target state $|\uparrow\rangle\langle\uparrow|$ in a time $t = O(1/\Gamma)$, the second spin has a slower dynamics described by a reduced effective Lindblad equation [28]. In fact, for $t \gg 1/\Gamma$ up to an error $O(1/\Gamma^2)$ we have $\rho(t) = |\uparrow\rangle\langle\uparrow| \otimes R(t)$ with $R(t)$ satisfying

$$\frac{\partial R}{\partial t} = -i[h_D, R] + \frac{1}{\Gamma}\left(\tilde{L}R\tilde{L}^\dagger - \tfrac{1}{2}(\tilde{L}^\dagger\tilde{L}R + R\tilde{L}^\dagger\tilde{L})\right), \quad (12)$$

where $h_D = \Delta\sigma^z$ and $\tilde{L} = 4(\sigma^x + i\gamma\sigma^y)$. Note that for $R(t)$, i.e., for the density matrix of the spin not directly affected by the dissipation, the effective dissipation strength is $1/\Gamma$ and not $\Gamma$ as in Eq. (1) for $\rho(t)$. The near Zeno limit NESS is

found straightforwardly as the time-independent solution of Eq. (12). This yields

$$\rho_{\text{Zeno}} = |\uparrow\rangle\langle\uparrow| \otimes \begin{pmatrix} \frac{(\gamma+1)^2}{2(\gamma^2+1)} & 0 \\ 0 & \frac{(\gamma-1)^2}{2(\gamma^2+1)} \end{pmatrix} + O\left(\frac{1}{\Gamma}\right). \quad (13)$$

To apply the near Zeno limit predictions, we must ensure that the $1/\Gamma$ Dyson perturbative expansion is convergent. Convergent series, which yield a unique sum, fail across branching points. Therefore, the $1/\Gamma$ Taylor series for each Liouvillian eigenvalue $\lambda_j$ is expected to have a convergence radius of $1/\Gamma_{\text{LEP}}(\lambda_j)$, where $\Gamma_{\text{LEP}}(\lambda_j)$ is the largest value of $\Gamma$ at which a branching point occurs (see Fig. 2). Beyond the critical point $\Gamma_{\text{cr}}$ defined above, *all* Liouvillian eigenvalues become analytic. On the $(\gamma, \Delta)$ plane, $\Gamma_{\text{cr}}$ is finite except near $\Delta = 0$ and $\gamma = 0$, where singularities appear. We find that $\Gamma_{\text{cr}}(\Delta)$ for $\Delta \to 0^+$ behaves as

$$\Gamma_{\text{cr}}(\Delta \to 0^+) = \max\left(\left|\frac{2(\gamma^2-1)}{\Delta}\right|, \left|\frac{\gamma^3 - 1/\gamma}{\Delta}\right|\right). \quad (14)$$

This singularity originates from the fact that at $\Delta = 0$ the spectrum of the dissipation projected Hamiltonian $h_D = \Delta\sigma^z$ becomes degenerate.

*Conclusions.* We analytically investigated the Liouvillian spectrum of two-qubits systems and identified regions of the LEPM where it is possible to achieve an effective Zeno regime at a minimal, $\Gamma_{\text{cr}}$, dissipation. We provided an analytic description of the temporal dynamics which applies in this regime and showed that the fastest relaxation time to the NESS occurs precisely on the LEPMs characterizing the effective Zeno regime. The rich LEPM structure uncovered here could be checked experimentally by quantum process tomography, as done in Ref. [29].

*Acknowledgment.* V.P. acknowledges support by ERC Advanced Grant No. 101096208–QUEST, and Research Programme No. P1-0402 of Slovenian Research and Innovation Agency (ARIS), and from Deutsche Forschungsgemeinschaft through DFG Project No. KL645/20-2.

*Data availability.* The data that support the findings of this article are not publicly available upon publication because it is not technically feasible and/or the cost of preparing, depositing, and hosting the data would be prohibitive within the terms of this research project. The data are available from the authors upon reasonable request.

[1] T. Kato, *A Short Introduction to Perturbation Theory for Linear Operators* (Springer, New York, 1982).
[2] W. D. Heiss, The physics of exceptional points, J. Phys. A: Math. Theor. **45**, 444016 (2012).
[3] M. A. Miri and A. Alù, Exceptional points in optics and photonics, Science **363**, eaar7709 (2019).
[4] J. Wiersig, Review of exceptional point-based sensors, Photon. Res. **8**, 1457 (2020).
[5] D. Anderson, M. Shah, and L. Fan, Clarification of the exceptional-point contribution to photonic sensing, Phys. Rev. Appl. **19**, 034059 (2023).
[6] M. Yang, L. Zhu, Q. Zhong, R. El-Ganainy, and P.-Y. Chen, Spectral sensitivity near exceptional points as a resource for hardware encryption, Nat. Commun. **14**, 1145 (2023).
[7] J.-W. Zhang, J.-Q. Zhang, G.-Y. Ding, J.-C. Li, J.-T. Bu, B. Wang, L.-L. Yan, S.-L. Su, L. Chen, F. Nori, Ş. K. Özdemir, F. Zhou, H. Jing, and M. Feng, Dynamical control of quantum heat engines using exceptional points, Nat. Commun. **13**, 6225 (2022).
[8] I. I. Arkhipov, A. Miranowicz, F. Minganti, Ş. K. Özdemir, and F. Nori, Dynamically crossing diabolic points while encircling exceptional curves: A programmable symmetric-asymmetric multimode switch, Nat. Commun. **14**, 2076 (2023).
[9] A. Li, H. Wei, M. Cotrufo, W. Chen, S. Mann, X. Ni, B. Xu, J. Chen, J. Wang, S. Fan, C.-W. Qiu, A. Alù, and L. Chen, Exceptional points and non-Hermitian photonics at the nanoscale, Nat. Nanotechnol. **18**, 706 (2023).
[10] G. Lindblad, On the generators of quantum dynamical semigroups, Commun. Math. Phys. **48**, 119 (1976).
[11] V. Gorini, A. Kossakowski, and E. C. G. Sudarshan, Completely positive dynamical semigroups of $N$-level systems, J. Math. Phys. **17**, 821 (1976).
[12] H.-P. Breuer and F. Petruccione, *The Theory of Open Quantum Systems* (Oxford University Press, Oxford, UK, 2002).
[13] F. Minganti, A. Miranowicz, R. W. Chhajlany, and F. Nori, Quantum exceptional points of non-Hermitian Hamiltonians and Liouvillians: The effects of quantum jumps, Phys. Rev. A **100**, 062131 (2019).
[14] J. Xu and Y. Guo, Unconventional steady states and topological phases in an open two-level non-Hermitian system, New J. Phys. **24**, 053028 (2022).
[15] O. A. D. Molitor, Jr., A. H. A. Malavazi, R. D. Baldijão, A. C. Orthey, Jr., I. L. Paiva, and P. R. Dieguez, Quantum switch instabilities with an open control, Commun. Phys. **7**, 373 (2024).
[16] N. Seshadri, A. Li, and M. Galperin, Liouvillian exceptional points of an open driven two-level system, J. Chem. Phys. **160**, 044116 (2024).
[17] Y.-L. Zhou, X.-D. Yu, C.-W. Wu, X.-Q. Li, J. Zhang, W. Li, and P.-X. Chen, Accelerating relaxation through Liouvillian exceptional point, Phys. Rev. Res. **5**, 043036 (2023).
[18] M. Nakagawa, N. Kawakami, and M. Ueda, Exact Liouvillian spectrum of a one- dimensional dissipative Hubbard model, Phys. Rev. Lett. **126**, 110404 (2021).
[19] R. Toskovic, R. van den Berg, A. Spinelli, I. S. Eliens, B. van den Toorn, B. Bryant, J. S. Caux, and A. F. Otte, Atomic spin-chain realization of a model for quantum criticality, Nat. Phys. **12**, 656 (2016).
[20] W. Yue, Qi Wei, S. Kais, B. Friedrich, and D. Herschbach, Realization of Heisenberg models of spin systems with polar molecules in pendular states, Phys. Chem. Chem. Phys. **24**, 25270 (2022).
[21] T. Villazon, P. W. Claeys, A. Polkovnikov, and A. Chandran, Shortcuts to dynamic polarization, Phys. Rev. B **103**, 075118 (2021).
[22] M. Knap, D. A. Abanin, and E. Demler, Dissipative dynamics of a driven quantum spin coupled to a bath of ultracold fermions, Phys. Rev. Lett. **111**, 265302 (2013).

[23] Given the matrix $A = [A_{ij}]_{i,j=1}^{n}$ we define the column vector $\mathrm{vec}(A) = (A_{11}, \ldots, A_{1n}, \ldots, A_{n1}, \ldots, A_{nn})^{\mathrm{T}}$, where $(\cdot)^{\mathrm{T}}$ indicates matrix transpose. This implies $\mathrm{vec}(AB) = (A \otimes I_n)\mathrm{vec}(B) = (B^{\mathrm{T}} \otimes I_n)\mathrm{vec}(A)$ and $\mathrm{vec}(ABC) = (A \otimes C^{\mathrm{T}})\mathrm{vec}(B)$, with $A, B, C$ arbitrary $n \times n$ matrices.

[24] See Supplemental Material at http://link.aps.org/supplemental/10.1103/PhysRevA.111.L050202 for mathematical details not appearing in the main text.

[25] We restrict to real parameters to keep contact with realistic physical settings, however, LEPMs exist for complex values of parameters as well.

[26] K. Kanki, S. Garmon, S. Tanaka, and T. Petrosky, Exact description of coalescing eigenstates in open quantum systems in terms of microscopic Hamiltonian dynamics, J. Math. Phys. **58**, 092101 (2017).

[27] V. Popkov and C. Presilla, Full spectrum of the Liouvillian of open dissipative quantum systems in the Zeno limit, Phys. Rev. Lett. **126**, 190402 (2021).

[28] V. Popkov, S. Essink, C. Presilla, and G. Schütz, Effective quantum Zeno dynamics in dissipative quantum systems, Phys. Rev. A **98**, 052110 (2018).

[29] S. Abo, P. Tulewicz, K. Bartkiewicz, S. K. Özdemir, and A. Miranowicz, Experimental Liouvillian exceptional points in a quantum system without Hamiltonian singularities, New J. Phys. **26**, 123032 (2024).

# Supplemental Material: Manifolds of exceptional points and effective Zeno limit of an open two-qubit system

Vladislav Popkov,[1,2] Carlo Presilla,[3,4] and Mario Salerno[5]
[1] *Faculty of Mathematics and Physics, University of Ljubljana, Jadranska 19, SI-1000 Ljubljana, Slovenia*
[2] *Bergisches Universität Wuppertal, Gauss Str. 20, D-42097 Wuppertal, Germany*
[3] *Dipartimento di Matematica, Sapienza Università di Roma, Piazzale A. Moro 5, 00185 Rome, Italy*
[4] *Istituto Nazionale di Fisica Nucleare, Sezione di Roma 1, 00185 Rome, Italy*
[5] *Dipartimento di Fisica "E.R. Caianiello", Università di Salerno, Via Giovanni Paolo II, 84084 Fisciano (SA), Italy*

This Supplemental Material contains eight sections organized as follows. In section A we describe the block structure $\Sigma_+, \Sigma_-$ of the Liouvillian. The polynomial equation whose roots provide the LEPs arising from $\Sigma_-$ is detailed in section B. In C we show some two-dimensional sections of the three-dimensional LEPMs given in Fig. 3 as well as of $\Gamma_{cr}(\gamma, \Delta)$ given in Fig. 4. The bifurcation diagrams at the four points indicated in Fig. 4 of the main text is shown in section D. In section E we explain how the boundary red line shown in Fig. 4 is obtained while in section F we make explicit the non-diagonalizability of the Liouvillian on the LEPMs. In section G we compare relaxation times to the NESS achieved on and out the $\Gamma = 8\gamma$ LEPM. Finally, in section G we discuss some subtle details regarding quantum Zeno regime which did not appear in the main text.

## A. Block diagonalization of the Liouvillian

The $\mathcal{Z}_2$ symmetry discussed in the main text allows to put the Liouvillian in the form

$$\mathcal{L} = \begin{pmatrix} \Sigma_+ & 0 \\ 0 & \Sigma_- \end{pmatrix}, \tag{S-1}$$

with the two $8 \times 8$ diagonal-blocks, $\Sigma_\pm$, related to the $\mathcal{Z}_2$ symmetry, achieved by eliminating the eight null rows and columns from the corresponding $16 \times 16$ matrices $\Sigma_\pm = \mathcal{U}_\pm \cdot \mathcal{L} \cdot \mathcal{U}_\pm$. In Fig. S-1 we show the block structure of the Liouvillian $\mathcal{L}$ obtained directly from Eq. (3) (left panel) and the one obtained after the $\mathcal{Z}_2$ block diagonalization discussed in the main text (right panel).

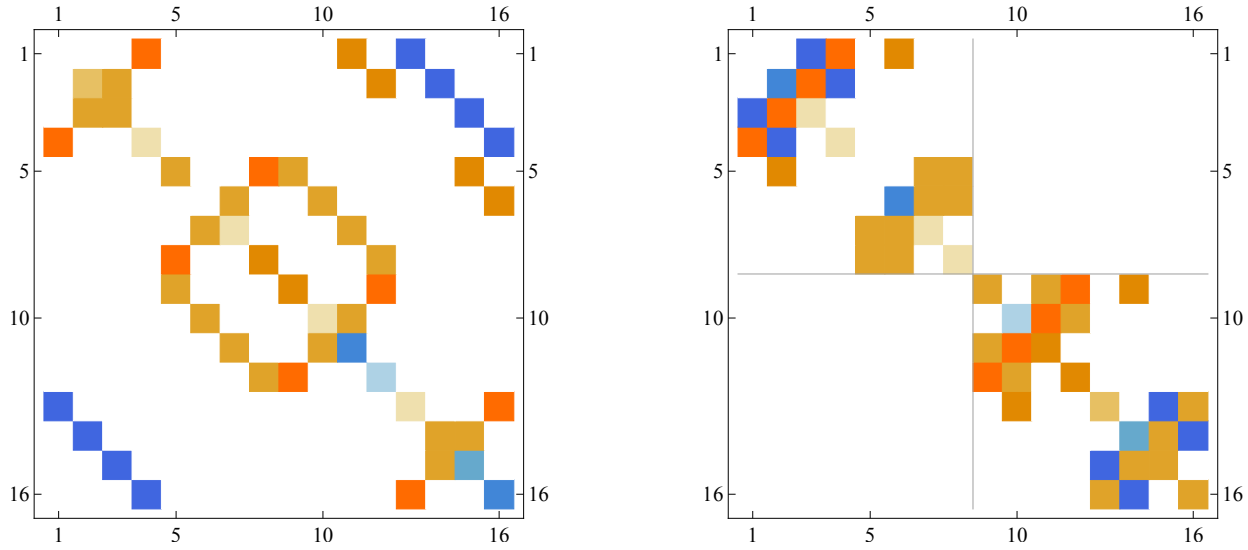


FIG. S-1: Liouvillian of the dissipative two qubit system as obtained from Eq. 3 (left panel) and its block diagonal form (right panel) acquired after operating the $\mathcal{U}_\pm$ transformation. Colors are associated to different matrix elements, white regions corresponding to zeros (for other color correspondences see Eqs. S-3, S-4).

The blocks $\Sigma_\pm$ can be further rearranged in the form

$$\Sigma_+ = \begin{pmatrix} A_1 & C \\ C & A_2 \end{pmatrix}, \qquad \Sigma_- = \begin{pmatrix} B_1 & C \\ C & B_2 \end{pmatrix} \tag{S-2}$$

with $C$ a $4\times 4$ matrix whose single nonzero element is $C_{1,2}=\Gamma$, and $A_1, A_2$ and $B_1, B_2$ are given by:

$$A_1 = \begin{pmatrix} 0 & 0 & -i(1-\gamma) & i(1-\gamma) \\ 0 & -\Gamma & i(1-\gamma) & -i(1-\gamma) \\ -i(1-\gamma) & i(1-\gamma) & -\frac{\Gamma}{2} & 0 \\ i(1-\gamma) & -i(1-\gamma) & 0 & -\frac{\Gamma}{2} \end{pmatrix},$$

$$A_2 = \begin{pmatrix} 0 & 0 & i(\gamma+1) & -i(\gamma+1) \\ 0 & -\Gamma & -i(\gamma+1) & i(\gamma+1) \\ i(\gamma+1) & -i(\gamma+1) & -\frac{\Gamma}{2} & 0 \\ -i(\gamma+1) & i(\gamma+1) & 0 & -\frac{\Gamma}{2} \end{pmatrix}, \tag{S-3}$$

$$B_1 = \begin{pmatrix} 2i\Delta & 0 & -i(\gamma+1) & i(1-\gamma) \\ 0 & -\Gamma+2i\Delta & i(1-\gamma) & -i(\gamma+1) \\ -i(\gamma+1) & i(1-\gamma) & -\frac{\Gamma}{2}+2i\Delta & 0 \\ i(1-\gamma) & -i(\gamma+1) & 0 & -\frac{\Gamma}{2}+2i\Delta \end{pmatrix},$$

$$B_2 = \begin{pmatrix} -2i\Delta & 0 & -i(1-\gamma) & i(\gamma+1) \\ 0 & -\Gamma-2i\Delta & i(\gamma+1) & -i(1-\gamma) \\ -i(1-\gamma) & i(\gamma+1) & -\frac{\Gamma}{2}-2i\Delta & 0 \\ i(\gamma+1) & -i(1-\gamma) & 0 & -\frac{\Gamma}{2}-2i\Delta \end{pmatrix}. \tag{S-4}$$

Note that the parameter $\Delta$ appears only in the block $\Sigma_-$.

From the above expressions it is easy to find that the secular equation for the eigenvalues of the block $\Sigma_+$ provides

$$\lambda(\Gamma+\lambda)(\Gamma+2\lambda)^2\Lambda(\gamma,\Gamma)=0, \tag{S-5}$$

where $\Lambda(\gamma,\Gamma)$ is the quartic polynomial in $\lambda$

$$\Lambda(\gamma,\Gamma)=\lambda^4+2\Gamma\lambda^3+\left[8(1+\gamma^2)+\frac{5}{4}\Gamma^2\right]\lambda^2+\left[8(1+\gamma^2)\Gamma+\frac{\Gamma^3}{4}\right]\lambda+2\left[8(1+\gamma^4)+\Gamma^2+\gamma^2(\Gamma^2-16)\right]. \tag{S-6}$$

We conclude that the eight $\Delta$-independent eigenvalues of $\Sigma_+$ are

$$\lambda(\gamma,\Gamma)=\left\{0,\,-\Gamma,\,-\frac{\Gamma}{2},\,-\frac{\Gamma}{2},\,-\frac{\Gamma}{2}\pm\frac{\sqrt{2}}{4}\sqrt{\Gamma^2-32(1+\gamma^2)\pm\sqrt{(\Gamma^2-64)(\Gamma^2-64\gamma^2)}}\right\}. \tag{S-7}$$

On the other hand, the eight $\Delta$-dependent eigenvalues of the block $\Sigma_-$ are given by

$$\lambda=\frac{1}{2}\left(-\Gamma\pm\sqrt{\Gamma^2+\xi_i}\right), \qquad i=1,\ldots,4, \tag{S-8}$$

where $\xi_i=\xi_i(\gamma,\Delta,\Gamma)$ are the roots of the quartic polynomial $c_a\xi^4+c_b\xi^3+c_c\xi^2+c_d\xi+c_e=0$ with coefficients

$$\begin{aligned}
c_a &= 1,\\
c_b &= 2\Gamma^2+2^5(1+\gamma^2)+2^6\Delta^2,\\
c_c &= 2^5\Gamma^2\left(2(1+\gamma^2)+5\Delta^2\right)+\Gamma^4+2^8\left(2\gamma^4+(1+\gamma^2)^2+2(1+\gamma^2)\Delta^2+6\Delta^4\right),\\
c_d &= 2^5\left(8\Gamma^2\left((1+\gamma^2)^2+6\gamma^2+14\Delta^4\right)+\Gamma^4\left((1+\gamma^2)+5\Delta^2\right)\right.\\
&\quad \left.+2^8\left(\gamma^2(1+\gamma^2)+\left((1+\gamma^2)^2-6\gamma^2\right)\Delta^2-(1+\gamma^2)\Delta^4+2\Delta^6\right)\right),\\
c_e &= 2^6\Gamma^6\Delta^2+2^{16}\left(\gamma^2-(1+\gamma^2)\Delta^2+\Delta^4\right)^2+2^8\Gamma^4\left(4\gamma^2-2(1+\gamma^2)\Delta^2+9\Delta^4\right)\\
&\quad +2^{12}\Gamma^2\left(2\gamma^2(1+\gamma^2)+\left((1+\gamma^2)-6\gamma^2\right)\Delta^2-4(1+\gamma^2)\Delta^4+6\Delta^6\right).
\end{aligned} \tag{S-9}$$

By using Mathematica, we find

$$\begin{aligned}
\xi_1 &= -c_b/(4c_a) - p_4/2 - \sqrt{p_5 - p_6}/2,\\
\xi_2 &= -c_b/(4c_a) - p_4/2 + \sqrt{p_5 - p_6}/2,\\
\xi_3 &= -c_b/(4c_a) + p_4/2 - \sqrt{p_5 + p_6}/2,\\
\xi_4 &= -c_b/(4c_a) - p_4/2 + \sqrt{p_5 + p_6}/2,
\end{aligned} \tag{S-10}$$

where

$$\begin{aligned}
p_1 &= 2c_c^3 - 9c_b c_c c_d + 27c_a c_d^2 + 27c_b^2 c_e - 72c_a c_c c_e,\\
p_2 &= p_1 + \sqrt{p_1^2 - 4(c_c^2 - 3c_b c_d + 12c_a c_e)^3},\\
p_3 &= (c_c^2 - 3c_b c_d + 12c_a c_e)/(3c_a \sqrt[3]{p_2/2}) + \sqrt[3]{p_2/2}/(3c_a),\\
p_4 &= \sqrt{c_b^2/(4c_a^2) - 2c_c/(3c_a) + p_3},\\
p_5 &= c_b^2/(2c_a^2) - 4c_c/(3c_a) - p_3,\\
p_6 &= (-c_b^3/c_a^3 + 4c_b c_c/c_a^2 - 8c_d/c_a)/(4p_4).
\end{aligned} \tag{S-11}$$

Note that with $\sqrt[3]{p_2/2}$ we mean the real-valued cube root of $p_2/2$.

### B. Polynomial equation for the LEP manifolds arising from $\Sigma_-$

All Liouvillian exceptional points (LEPs) in the $(\gamma, \Delta, \Gamma)$ parameter space of the $\Sigma_-$ block are determined by requiring that the discriminant of the polynomial in Eq. (9) vanishes. This condition yields the following degree-eight polynomial equation in the $Z \equiv \Gamma^2$ variable

$$\sum_{i=0}^{8} a_i(X, Y) Z^i = 0, \tag{S-12}$$

with coefficients $a_i$ given by

$$\begin{aligned}
a_0 &= 2^{32}(X-1)^4 XY^2(X^2 + (1-4Y)^2 - 2X(1+4Y))^2,\\
a_1 &= -2^{27}(X-1)^8 XY + 2^{31}(X-1)^6(X+1)XY^2 + 2^{31}(X-1)^4(1+30X+X^2)XY^3\\
&\quad - 2^{35}(X-1)^2 X(X+1)(3+2X+3X^2)Y^4 + 2^{36}(X-1)^2 X(5+6X+5X^2)Y^5 - 2^{38}X(X-1)^2(X+1)Y^6,\\
a_2 &= 2^{20}(-1+X)^8 X + 2^{20}(-1+X)^6(1+X)(1-34X+X^2)Y - 2^{23}(-1+X)^4(1+24X+238X^2+24X^3+X^4)Y^2\\
&\quad + 2^{24}(-1+X)^2(1+X)(1+44X-602X^2+44X^3+X^4)Y^3 + 2^{29}X(27+36X+2X^2+36X^3+27X^4)Y^4\\
&\quad - 2^{33}X(1+X)(5-2X+5X^2)Y^5 + 2^{33}X(3+2X+3X^2)Y^6,\\
a_3 &= -2^{14}(-1+X)^6(1+X)(1-18X+X^2) + 2^{18}(-1+X)^4(1+4X+54X^2+4X^3+X^4)Y\\
&\quad + 2^{21}(1+X)(-1+X)^2(1+10X+42X^2+10X^3+X^4)Y^2 - 2^{20}(3+22X-883X^2-332X^3\\
&\quad - 883X^4+22X^5+3X^6)Y^3 - 2^{26}X(1+X)(21+22X+21X^2)Y^4 + 2^{29}X(5+6X+5X^2)Y^5 - 2^{30}X(1+X)Y^6,\\
a_4 &= -2^8(-1+X)^4(15-60X-166X^2-60X^3+15X^4) - 2^{15}(-1+X)^2(1+X)(1+4X-42X^2+4X^3+X^4)Y\\
&\quad - 2^{16}(3+42X-3X^2-340X^3-3X^4+42X^5+3X^6)Y^2 + 2^{16}(1+X)(3-156X-974X^2-156X^3+3X^4)Y^3\\
&\quad + 2^{21}X(39+74X+39X^2)Y^4 - 5\times 2^{24}X(1+X)Y^5 + 2^4 XY^6,\\
a_5 &= -2^6(3+X-21X^2+17X^3+17X^4-21X^5+X^6+3X^7) - 2^8(-1+X)^2(1+68X+246X^2+68X^3+X^4)Y\\
&\quad + 2^{13}(1+X)(1-6X+X^2)(1+14X+X^2)Y^2 - 2^{12}(1-236X-682X^2-236X^3+X^4)Y^3\\
&\quad - 9\times 2^{18}X(1+X)Y^4 + 2^{20}XY^5,\\
a_6 &= 2^2(1-2X-X^2+4X^3-X^4-2X^5+X^6) + 2^4(-1+X)^2(1+X)(5+38X+5X^2)Y\\
&\quad - 2^7(1-28X-138X^2-28X^3+X^4)Y^2 - 7\times 2^{12}X(1+X)Y^3 + 3\times 2^{13}XY^4,\\
a_7 &= -(1+4X-10X^2+4X^3+X^4)Y - 2^7X(1+X)Y^2 + 2^8XY^3,
\end{aligned}$$

$a_8 = XY^2$.

It is worth noting the multi-polynomial structure of Eq. (S-1), where the coefficients $a_i$ are polynomials in $Y = \Delta^2$, whose coefficients are, in turn, polynomials in $X = \gamma^2$. This nested polynomial structure reveals the complexity of the LEPMs in the parameter space.

### C. Two-dimensional cuts of the LEP manifolds

In Fig. S-2 we show the two-dimensional sections at $\Delta = 0.8$ (left panel) and $\gamma = 1.5$ (right panel) of the three-dimensional LEP manifolds reported in Fig. 3. The solid blue lines are the sections of the $\Delta$-dependent LEPs arising from $\Sigma_-$ while the dashed lines indicates the LEPs $\Gamma = 8$ and $\Gamma = 8\gamma$ from the $\Delta$-independent Liouvillian block $\Sigma_+$.

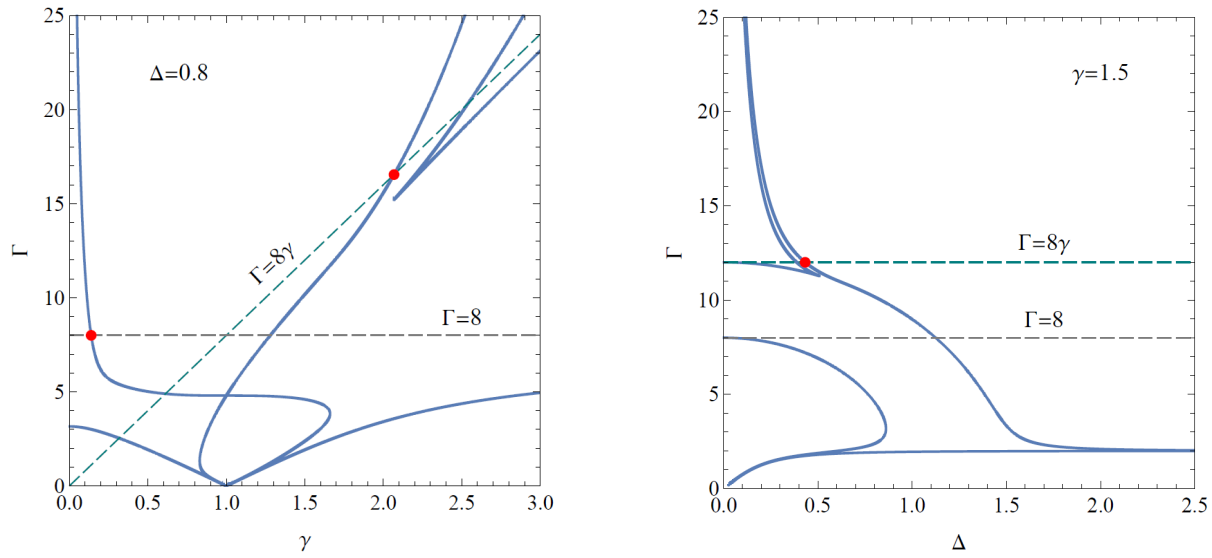


FIG. S-2: Two-dimensional sections at $\Delta = 0.8$ (left panel) and $\gamma = 1.5$ (right panel) of the manifolds shown in Fig. 3. The dashed straight lines indicate the intersections with the $\Gamma = 8$ and $\Gamma = 8\gamma$ planes (not shown in Fig. 3).

In Fig. S-3 we provide the two-dimensional sections at $\Delta = 0.1$, 03, and 0.7 of $\Gamma_{cr}(\gamma, \Delta)$ given in Fig. 4. Also in this case, the dashed lines are the sections of the planes $\Gamma = 8$ and $\Gamma = 8\gamma$ which partially coincide with the $\Delta$-dependent sections shown by solid lines.

### D. Bifurcation diagrams at points a,b,c,d in Fig. 4 of the main text

In Fig. S-4 we depict the bifurcation diagrams obtained for the rescaled real part of all Liouvillian eigenvalues (from $\Sigma_-$ as well as from $\Sigma_+$) as a function of $\Gamma$ for parameter values corresponding to points a, b, c, d of Fig. 4. In cases a,d the largest bifurcation belongs to the $\Delta$-dependent Liouvillian eigenvalues (red curves), while in cases b,c it belongs to the $\Delta$-independent Liouvillian eigenvalues (blue curves), in full agreement with the analysis done in the main text, see Fig. 4.

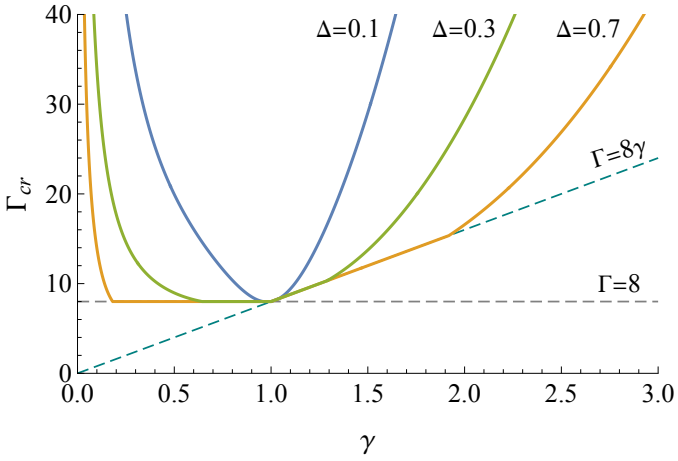


FIG. S-3: Two-dimensional sections at $\Delta = 0.1$, 03, and 0.7 of $\Gamma_{cr}(\gamma, \Delta)$ of Fig. 4. The dashed lines are the sections of the planes $\Gamma = 8$ and $\Gamma = 8\gamma$.

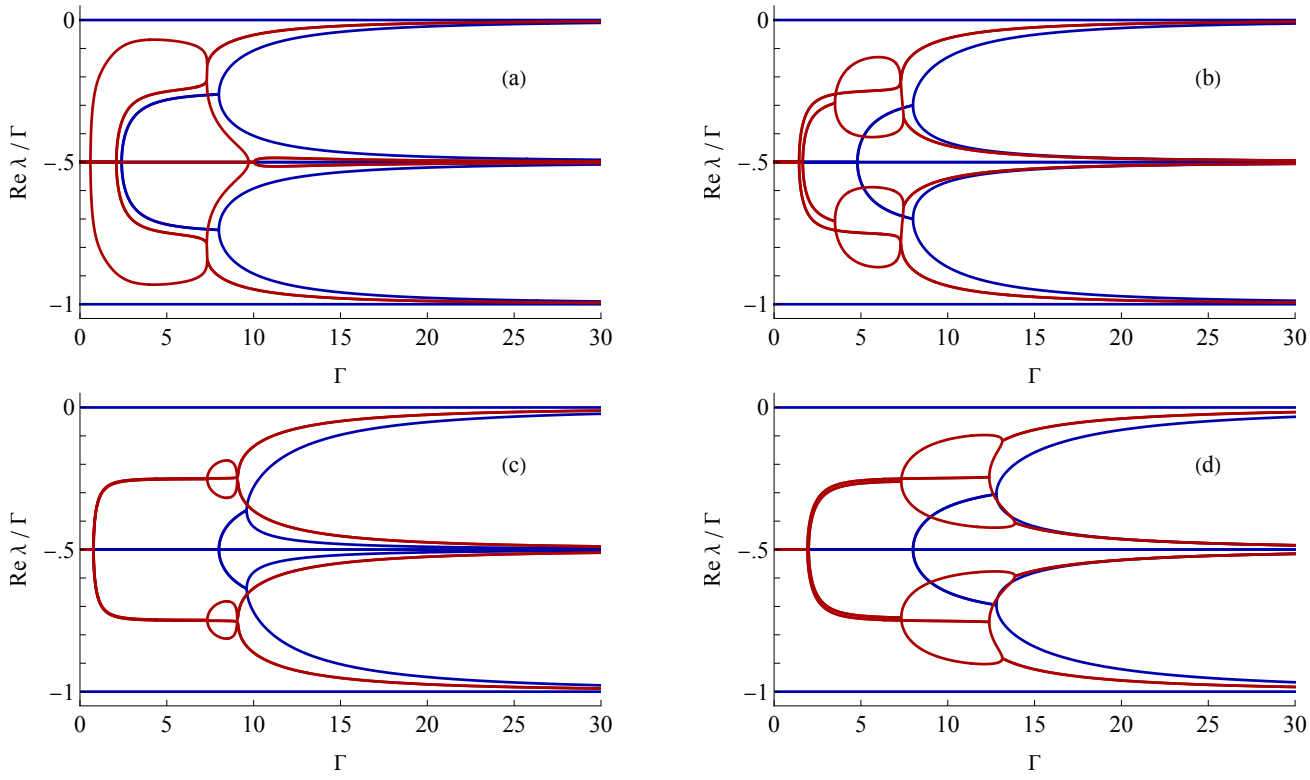


FIG. S-4: Rescaled real parts of the Liouvillian eigenvalues versus $\Gamma$ for parameter values $(\gamma, \Delta) = (0.3, 0.4)$, $(0.6, 0.4)$, $(1.2, 0.4)$, and $(1.6, 0.4)$ corresponding, respectively, to the points a,b,c, and d depicted in Fig. 4 of the main text. Blue and red dots refer to $\Delta$-independent and $\Delta$-dependent eigenvalues, respectively. Notice that for the $\Delta$-independent part of the spectrum the first and second left most branching points occur at $\Gamma = \min(8, 8\gamma)$ and at $\Gamma = \max(8, 8\gamma)$, respectively.

### E. Obtaining the boundary lines in Fig. 4

Here we explain how we obtain the red boundary lines, shown in both panels of Fig. 4, separating the regions where $\Gamma_{cr}$ corresponds to a LEP arising from an eigenvalue of $\Sigma_+$ or $\Sigma_-$.

To determine the left part of the curve, we solve numerically Eq. (S-1) for $\Delta$ fixing the value of $\Gamma = 8$ and varying $\gamma$ in the interval $0 < \gamma < 1$. This yields two branches of solutions $\Delta_{1L}(\gamma) > 0$ and $\Delta_{2L}(\gamma) > \Delta_{1L}(\gamma)$. The upper branch $\Delta_{2L}y(\gamma)$ gives the red line in Fig. 4 in the interval $0 < \gamma < 1$.

| $-8$ | $-4$ | $-4$ | $0$ | $2(-2+\sqrt{1-\gamma^2})$ | $2(-2+\sqrt{1-\gamma^2})$ | $-2(2+\sqrt{1-\gamma^2})$ | $-2(2+\sqrt{1-\gamma^2})$ |
|---|---|---|---|---|---|---|---|
| $-1$ | $0$ | $0$ | $\frac{i(1+\gamma)(17-2\gamma+\gamma^2)}{4(-1+\gamma)^2}$ | $-\frac{i(4+4\gamma+3\sqrt{1-\gamma^2}+\gamma\sqrt{1-\gamma^2})}{(1+\gamma)(2+\sqrt{1-\gamma^2})}$ | $0$ | $-\frac{i(-4-4\gamma+3\sqrt{1-\gamma^2}+\gamma\sqrt{1-\gamma^2})}{(1+\gamma)(-2+\sqrt{1-\gamma^2})}$ | $0$ |
| $-1$ | $0$ | $0$ | $\frac{1}{4}i(1+\gamma)$ | $\frac{i(-\sqrt{1-\gamma^2}+\gamma\sqrt{1-\gamma^2})}{(1+\gamma)(2+\sqrt{1-\gamma^2})}$ | $0$ | $\frac{i(-\sqrt{1-\gamma^2}+\gamma\sqrt{1-\gamma^2})}{(1+\gamma)(-2+\sqrt{1-\gamma^2})}$ | $0$ |
| $0$ | $0$ | $1$ | $-\frac{1+\gamma}{-1+\gamma}$ | $-\frac{1-\gamma}{\sqrt{1-\gamma^2}}$ | $0$ | $-\frac{-1+\gamma}{\sqrt{1-\gamma^2}}$ | $0$ |
| $0$ | $0$ | $1$ | $-\frac{-1-\gamma}{-1+\gamma}$ | $-\frac{-1+\gamma}{\sqrt{1-\gamma^2}}$ | $0$ | $-\frac{1-\gamma}{\sqrt{1-\gamma^2}}$ | $0$ |
| $1$ | $0$ | $0$ | $\frac{i(17+2\gamma+\gamma^2)}{4(1+\gamma)}$ | $\frac{2i\sqrt{1-\gamma^2}}{1+\gamma}+\frac{i(1+\gamma)}{2+\sqrt{1-\gamma^2}}$ | $0$ | $\frac{i(-3-2\gamma+\gamma^2+4\sqrt{1-\gamma^2})}{(1+\gamma)(-2+\sqrt{1-\gamma^2})}$ | $0$ |
| $1$ | $0$ | $0$ | $\frac{1}{4}i(1+\gamma)$ | $\frac{i(1+\gamma)}{2+\sqrt{1-\gamma^2}}$ | $0$ | $-\frac{i(1+\gamma)}{-2+\sqrt{1-\gamma^2}}$ | $0$ |
| $0$ | $1$ | $0$ | $-1$ | $-1$ | $0$ | $-1$ | $0$ |
| $0$ | $1$ | $0$ | $1$ | $1$ | $0$ | $1$ | $0$ |

TABLE I: Eigenvalues (top row) and eigenvectors (corresponding underlying columns) of the $\Sigma_+$ diagonal block of the Liouvillian on the LEPM $\{\gamma, \Delta, \Gamma = 8\}$.

| $0$ | $-8\gamma$ | $-4\gamma$ | $-4\gamma$ | $2(\sqrt{\gamma^2-1}-2\gamma)$ | $2(\sqrt{\gamma^2-1}-2\gamma)$ | $-2(\sqrt{\gamma^2-1}+2\gamma)$ | $-2(\sqrt{\gamma^2-1}+2\gamma)$ |
|---|---|---|---|---|---|---|---|
| $\frac{i(1+\gamma)(1-2\gamma+17\gamma^2)}{4(-1+\gamma)^2\gamma}$ | $-1$ | $0$ | $0$ | $-\frac{i(4\gamma+4\gamma^2+\sqrt{-1+\gamma^2}+3\gamma\sqrt{-1+\gamma^2})}{(1+\gamma)(2\gamma+\sqrt{-1+\gamma^2})}$ | $0$ | $-\frac{i(4\gamma+4\gamma^2-\sqrt{-1+\gamma^2}-3\gamma\sqrt{-1+\gamma^2})}{(1+\gamma)(2\gamma-\sqrt{-1+\gamma^2})}$ | $0$ |
| $\frac{i(1+\gamma)}{4\gamma}$ | $-1$ | $0$ | $0$ | $-\frac{i(-\sqrt{-1+\gamma^2}+\gamma\sqrt{-1+\gamma^2})}{(1+\gamma)(2\gamma+\sqrt{-1+\gamma^2})}$ | $0$ | $-\frac{i(-\sqrt{-1+\gamma^2}+\gamma\sqrt{-1+\gamma^2})}{(1+\gamma)(-2\gamma+\sqrt{-1+\gamma^2})}$ | $0$ |
| $-\frac{1+\gamma}{-1+\gamma}$ | $0$ | $0$ | $1$ | $-\frac{1-\gamma}{\sqrt{-1+\gamma^2}}$ | $0$ | $-\frac{-1+\gamma}{\sqrt{-1+\gamma^2}}$ | $0$ |
| $-\frac{-1-\gamma}{-1+\gamma}$ | $0$ | $0$ | $1$ | $-\frac{-1+\gamma}{\sqrt{-1+\gamma^2}}$ | $0$ | $-\frac{1-\gamma}{\sqrt{-1+\gamma^2}}$ | $0$ |
| $\frac{i(1+2\gamma+17\gamma^2)}{4\gamma(1+\gamma)}$ | $1$ | $0$ | $0$ | $\frac{2i\sqrt{-1+\gamma^2}}{1+\gamma}+\frac{i(1+\gamma)}{2\gamma+\sqrt{-1+\gamma^2}}$ | $0$ | $-\frac{2i\sqrt{-1+\gamma^2}}{1+\gamma}-\frac{i(1+\gamma)}{-2\gamma+\sqrt{-1+\gamma^2}}$ | $0$ |
| $\frac{i(1+\gamma)}{4\gamma}$ | $1$ | $0$ | $0$ | $\frac{i(1+\gamma)}{2\gamma+\sqrt{-1+\gamma^2}}$ | $0$ | $-\frac{i(1+\gamma)}{-2\gamma+\sqrt{-1+\gamma^2}}$ | $0$ |
| $-1$ | $0$ | $1$ | $0$ | $-1$ | $0$ | $-1$ | $0$ |
| $1$ | $0$ | $1$ | $0$ | $1$ | $0$ | $1$ | $0$ |

TABLE II: As in Table I on the LEPM $\{\gamma, \Delta, \Gamma = 8\gamma\}$.

Likewise, in the region $1 < \gamma$ we solve Eq. (S-1) for $\Delta$, fixing the value of $\Gamma = 8\gamma$ and varying $\gamma > 1$. Also in this case we obtain two branches of solutions $\Delta_{1R}(\gamma) > 0$ and $\Delta_{2R}(\gamma) > \Delta_{1R}(\gamma)$. The upper branch $\Delta_{2R}(\gamma)$ gives the red line in Fig. 4 in the region $\gamma > 1$.

### F. Non-diagonalizability of the Liouvillian on LEPMs

In this section we show that on the LEPMs the Liouvillian matrix is non-diagonalizable. The analysis is made on the two diagonal blocks $\Sigma_\pm$, separately. For the block $\Sigma_+$ the LEPMs are $\Delta$ independent, they are the points of the two planes $\Gamma = 8$ and $\Gamma = 8\gamma$. Eigenvalues and eigenvectors of $\Sigma_+$ at these points are reported in Table I and II, respectively. In both cases, we note the presence of the null eigenvalue in the spectrum, meaning that the NESS of the system, obtained from the corresponding eigenvector, belongs to the block $\Sigma_+$.

From Tables I and II it is evident that the coalescence of two pairs of complex eigenvalues (5th-6th and 7th-8th eigenvalues in both tables) is associated to the appearance of two null eigenvectors in the corresponding eigenspace. In fact, the dimension of the eigenspace is reduced as in the general case of linearly dependent eigenvectors. In other words, the $\Sigma_+$ matrix becomes non-diagonalizable and its Jordan decomposition provides the typical Jordan blocks shown in Table III.

$$\Sigma_+(\gamma,\Delta,\Gamma=8)=\begin{pmatrix}
-8 & 0 & 0 & 0 & 0 & 0 & 0 & 0\\
0 & -4 & 0 & 0 & 0 & 0 & 0 & 0\\
0 & 0 & -4 & 0 & 0 & 0 & 0 & 0\\
0 & 0 & 0 & 0 & 0 & 0 & 0 & 0\\
0 & 0 & 0 & 0 & \alpha_+ & 1 & 0 & 0\\
0 & 0 & 0 & 0 & 0 & \alpha_+ & 0 & 0\\
0 & 0 & 0 & 0 & 0 & 0 & \alpha_- & 1\\
0 & 0 & 0 & 0 & 0 & 0 & 0 & \alpha_-
\end{pmatrix}
\qquad
\Sigma_+(\gamma,\Delta,\Gamma=8\gamma)=\begin{pmatrix}
0 & 0 & 0 & 0 & 0 & 0 & 0 & 0\\
0 & -8\gamma & 0 & 0 & 0 & 0 & 0 & 0\\
0 & 0 & -4\gamma & 0 & 0 & 0 & 0 & 0\\
0 & 0 & 0 & -4\gamma & 0 & 0 & 0 & 0\\
0 & 0 & 0 & 0 & \beta_+ & 1 & 0 & 0\\
0 & 0 & 0 & 0 & 0 & \beta_+ & 0 & 0\\
0 & 0 & 0 & 0 & 0 & 0 & \beta_- & 1\\
0 & 0 & 0 & 0 & 0 & 0 & 0 & \beta_-
\end{pmatrix}$$

TABLE III: Jordan block form of $\Sigma_+$ on the LEPMs relative to Table I (left matrix) and Table II (right matrix). We put $\alpha_\pm=-4\pm2\sqrt{1-(8\gamma)^2}$ and $\beta_\pm=-4\gamma\pm2\sqrt{\gamma^2-1}$.

| $-6-2i\Delta$ | $-6-2i\Delta$ | $-2-2i\Delta$ | $-2-2i\Delta$ | $-6+2i\Delta$ | $-6+2i\Delta$ | $-2+2i\Delta$ | $-2+2i\Delta$ |
|---|---|---|---|---|---|---|---|
| $\frac{-2\Delta+i}{(\Delta+i)^2}$ | 0 | 0 | 0 | 0 | 0 | $i$ | 0 |
| 0 | 0 | 0 | 0 | $i(\Delta+i)^2$ | 0 | 0 | 0 |
| $-\frac{1}{(\Delta+i)^2}$ | 0 | 0 | 0 | 0 | 0 | 1 | 0 |
| 0 | 0 | 0 | 0 | $-i(\Delta+i)^2$ | 0 | 0 | 0 |
| 0 | 0 | $-i$ | 0 | $2\Delta+i$ | 0 | 0 | 0 |
| $i$ | 0 | 0 | 0 | 0 | 0 | 0 | 0 |
| 1 | 0 | 0 | 0 | 0 | 0 | 0 | 0 |
| 0 | 0 | 1 | 0 | 1 | 0 | 0 | 0 |

TABLE IV: Eigenvalues and eigenvectors of the diagonal block $\Sigma_-$, arranged as in Table I, on the EP line $\{\gamma=1,\Delta,\Gamma=8\}$.

Similar results are obtained for the $\Sigma_-$ block of the Liouvillian. However, in the case of this $\Delta$-dependent block the LEPMs are much more involved with complicated topology and several sheets. Taking only positive real values for $\gamma,\Delta$ and restricting to only real positive solutions of the polynomial equation (S-1), one can show that LEPM can have a number of sheets (branches) that varies from 1 to 6 depending on the values of $\gamma,\Delta$.

Analytical expressions for the Jordan block decomposition of $\Sigma_-$, except for a few simple cases (see below), are impossible to derive and one must recourse to numerical calculations. Using numerical solutions of Eq. (S-1) one finds for generic points on a LEPM, results qualitatively similar to those obtained for the block $\Sigma_+$ with the difference that the NESS does not belong to the manifold and the number of pairs of complex coalescing eigenvalues can be maximal, i.e., as large as 4, depending on $\gamma,\Delta$ values.

A particularly simple case in which the coalescence of the eigenvalues and eigenvectors of the $\Sigma_-$ block can be checked analytically is obtained for $\gamma=1$. In this case the coefficients of the polynomial appearing in Eq. (S-1) drastically simplify and it admits the real positive root $\Gamma=8$ for all values of $\Delta$. The corresponding LEPM then becomes the EP line $\{\gamma=1,\Delta,\Gamma=8\}$. Eigenvalues and eigenvectors of the $\Sigma_-$ block along this line are reported in Table IV and the corresponding Jordan block decomposition is given in Table V.

$$\Sigma_-(\gamma=1,\Delta,\Gamma=8)=\begin{pmatrix}
-8-2i & 1 & 0 & 0 & 0 & 0 & 0 & 0\\
0 & -8-2i & 0 & 0 & 0 & 0 & 0 & 0\\
0 & 0 & -6+2i & 1 & 0 & 0 & 0 & 0\\
0 & 0 & 0 & -6+2i & 0 & 0 & 0 & 0\\
0 & 0 & 0 & 0 & -4-2i & 1 & 0 & 0\\
0 & 0 & 0 & 0 & 0 & -4-2i & 0 & 0\\
0 & 0 & 0 & 0 & 0 & 0 & -2+2i & 1\\
0 & 0 & 0 & 0 & 0 & 0 & 0 & -2+2i
\end{pmatrix}$$

TABLE V: Jordan block form of $\Sigma_-$ on the LEPMs $\{\gamma=1,\Delta,\Gamma=8\}$.

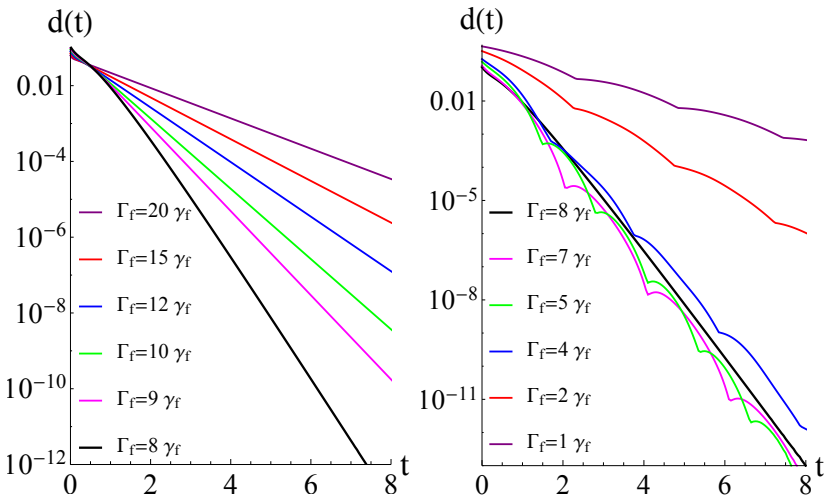


FIG. S-5: Distance $d(t) \equiv \|\rho(t) - \rho_{\rm NESS}(\gamma_f)\|_2$ versus time $t$ for rapid quenches in the parameter $\gamma$, from $\gamma_i = 1.1$ to $\gamma_f = 1.6$, on different $\Gamma = n\gamma$ planes as indicated in the legend, for arbitrary $\Delta$. The left panel shows data for planes above the $\Gamma = 8\gamma$ LEPM, while the right panel data for planes below it.

### G. Relaxation times near and on the $\Gamma = 8\gamma$ LEPM.

In the following, we show that in the region $\gamma > 1$ of the parameter space that characterizes the effective Zeno regime with $\Gamma_{cr} = 8\gamma$, the fastest relaxation from an initial perturbed state to the exact NESS is achieved on the $\Gamma = 8\gamma$ LEPM. In this case, the quench involves two parameters and is done from $\gamma_i, \Gamma_i = 8\gamma_i$ to $\gamma_f, \Gamma_f = 8\gamma_f$. The results obtained are depicted in Fig. S-5 from which we see that the fastest relaxation is achieved on the $\Gamma = 8\gamma$ plane.

### H. Convergence to NESS and characteristic dissipation value $\Gamma_{ch}$.

The exact NESS of the two-qubit problem (when it is unique) can be evaluated analytically and is given by

$$\rho_{\rm NESS}(\Gamma) = \begin{pmatrix} \frac{(\gamma+1)^2\left(4\gamma^2-8\gamma+\Gamma^2+4\right)}{2\left(8\gamma^4+\gamma^2\left(\Gamma^2-16\right)+\Gamma^2+8\right)} & 0 & 0 & -\frac{i(\gamma-1)(\gamma+1)^2\Gamma}{8\gamma^4+\gamma^2\left(\Gamma^2-16\right)+\Gamma^2+8} \\ 0 & \frac{(\gamma-1)^2\left(4\gamma^2+8\gamma+\Gamma^2+4\right)}{2\left(8\gamma^4+\gamma^2\left(\Gamma^2-16\right)+\Gamma^2+8\right)} & \frac{i(\gamma-1)^2(\gamma+1)\Gamma}{8\gamma^4+\gamma^2\left(\Gamma^2-16\right)+\Gamma^2+8} & 0 \\ 0 & -\frac{i(\gamma-1)^2(\gamma+1)\Gamma}{8\gamma^4+\gamma^2\left(\Gamma^2-16\right)+\Gamma^2+8} & \frac{2(\gamma-1)^2(\gamma+1)^2}{8\gamma^4+\gamma^2\left(\Gamma^2-16\right)+\Gamma^2+8} & 0 \\ \frac{i(\gamma-1)(\gamma+1)^2\Gamma}{8\gamma^4+\gamma^2\left(\Gamma^2-16\right)+\Gamma^2+8} & 0 & 0 & \frac{2(\gamma-1)^2(\gamma+1)^2}{8\gamma^4+\gamma^2\left(\Gamma^2-16\right)+\Gamma^2+8} \end{pmatrix}. \quad \text{(S-13)}$$

Note that the NESS is $\Delta$-independent. In the quantum Zeno limit we have

$$\rho_{\rm Zeno} = \lim_{\Gamma\to\infty} \rho_{\rm NESS}(\Gamma) = |\uparrow\rangle\langle\uparrow| \otimes \begin{pmatrix} \frac{(\gamma+1)^2}{2(\gamma^2+1)} & 0 \\ 0 & \frac{(\gamma-1)^2}{2(\gamma^2+1)} \end{pmatrix}, \quad \text{(S-14)}$$

in accordance with Eq. (13) obtained in the main text with the help of the reduced Zeno dynamics [28]. We observe that for large $\Gamma$

$$\mathrm{tr}(\rho^2_{\rm Zeno}) - \mathrm{tr}(\rho^2_{\rm NESS}(\Gamma)) = O\left(\frac{1}{\Gamma^2}\right) + \ldots \quad \text{(S-15)}$$

so that this quantity can serve as a measure of the distance to the Zeno NESS for fixed values of the dissipation $\Gamma$.

Using Eq. (S-3) we introduce a characteristic dissipation strength $\Gamma_{ch}$ needed to reach the Zeno NESS, as

$$\Gamma^2_{ch}(\gamma) = \lim_{\Gamma\to\infty} \Gamma^2 \left[\mathrm{tr}(\rho^2_{\rm Zeno}) - \mathrm{tr}(\rho^2_{\rm NESS}(\Gamma))\right] = \frac{4\gamma^{10} + 36\gamma^8 - 40\gamma^6 - 40\gamma^4 + 36\gamma^2 + 4}{\gamma^8 + 4\gamma^6 + 6\gamma^4 + 4\gamma^2 + 1}. \quad \text{(S-16)}$$

First of all, note that $\Gamma_{ch}$ is independent of $\Delta$ and also it does not have any singularities for $\gamma \to 0$. This might seem in contradiction to what is stated in Eq. (14). To resolve the issue, we remark that the effective dynamics (12) only concerns the relaxation of the diagonal elements of the reduced density matrix, i.e., those elements which in the limit $\Gamma \to \infty$ become the NESS eigenvalues. Expression (S-4) thus gives an estimate of the relaxation of a part of the system only, while for the relaxation of the non-diagonal part of the reduced density matrix $\rho$ the full system (1) still needs to be considered.